New Journal of Physics
An Institute of Physics and Deutsche Physikalische Gesellschaft Journal

Curvature effects on the structural, electronic and optical properties of isolated single-walled carbon nanotubes within a symmetry-adapted non-orthogonal tight-binding model

Valentin N Popov[1]

Laboratoire de Physique du Solide, Facultés Universitaires Notre-Dame de la Paix, Rue de Bruxelles, 61, B-5000 Namur, Belgium
E-mail: valentin.popov@fundp.ac.be

New Journal of Physics **6** (2004) 17
Received 30 June 2003
Published 5 February 2004
Online at http://www.njp.org/ (DOI: 10.1088/1367-2630/6/1/017)

Abstract. The effects of curvature on the structure, electronic and optical properties of isolated single-walled carbon nanotubes are studied within a symmetry-adapted non-orthogonal tight-binding model using 2s and 2p electrons of carbon. The symmetry-adapted scheme allows reducing the matrix eigenvalue problem for the electrons to diagonalization of 8×8 matrices for any nanotube type. Due to this simplification, the electronic band structure of nanotubes with a very large number of atoms in the unit cell can be calculated. Using this model, the structure of 187 small- and moderate-radius nanotubes is optimized. It is found that the deviations of the optimized structure from the non-optimized one are large for tube radii smaller than 5 Å. The band structure and the dielectric function of 101 small- and moderate-radius nanotubes are calculated. The optical transition energies for these nanotubes are derived from the dielectric function and plotted versus tube radius. It is shown that the structural optimization introduces small changes to the transition energies obtained within the non-orthogonal tight-binding model. The transition energies for the optimized structure within this model agree well with the available *ab initio* data for a few nanotube types. On the other hand, the results for the former deviate widely from those used for nanotube characterization in π-band tight-binding model especially for small-radius tubes. The derived transition energies can be used for the assignment of nanotube absorption spectra and for the selection of nanotube types for which the Raman scattering is resonant.

[1] Permanent address: University of Sofia, Faculty of Physics, 5 James Bourchier Blvd., BG-1164 Sofia, Bulgaria. E-mail: vpopov@phys.uni-sofia.bg

PII: S1367-2630(04)65456-5
© IOP Publishing Ltd and Deutsche Physikalische Gesellschaft

Contents

1. Introduction

The discovery of the carbon nanotubes in 1991 [1] and the speculations about their amazing electronic properties [2]–[4] directed much attention to their experimental and theoretical study. In the simplest case, a nanotube consists of a single graphitic layer and is termed a single-walled carbon nanotube (or, for brevity, a nanotube). A nanotube can be viewed as a long strip of a graphene sheet rolled up into a seamless cylindrical surface and can be characterized uniquely by a pair of non-negative integer numbers (L_1, L_2). Nanotubes with diameters equal to or greater than that of C_{60} are either metallic (zero-gap semiconducting) of the armchair type ($L_1 = L_2$), or small- or moderate-gap semiconductors ($L_1 \neq L_2$). In [2] it is shown that all armchair tubes are metallic in the presence of curvature and stable against a spontaneous symmetry breaking to far below room temperature. Hamada *et al* [3] used the graphene sheet model introduced in [2] together with all-valence tight-binding (TB) calculations for zigzag nanotubes ($L_1 \neq 0, L_2 = 0$) to show that nanotubes other than armchair should be either small- or moderate-gap semiconductors. Saito *et al* [4] applied the graphene sheet model in π-band tight-binding (π-TB) calculations to predict that nanotubes with $L_1 - L_2$ which is equal to a multiple of 3 are metallic instead of small-gap ones. Extensive band structure calculations for nanotubes were carried out using an all-valence TB approach and a first-principles all-electron density-functional-theory approach within the local density approximation (LDA) [5] based on a symmetry-adapted scheme [6]. Detailed plane-wave *ab initio* pseudopotential LDA calculations of small-radius insulating nanotubes [7] showed that strongly modified low-lying non-degenerate conduction band states are introduced into the band gap due to σ^*–π^* rehybridization. As a result, the LDA gaps of some tubes are lowered by more than 50% and the tube (6, 0) previously predicted to be semiconducting within the all-valence TB models is shown to be metallic. Similar effects were observed in the electronic properties of carbon nanotubes with polygonized cross sections calculated within a plane-wave *ab initio* pseudopotential LDA approach [8]. Recently, in an extensive *ab initio* LDA study of nanotubes with radii between 5 and 7.5 Å, a shift of the electron eigenenergies up to ~0.1 eV relative to the results of the π-TB model was predicted [9].

The optical properties of nanotubes have been treated exclusively within π-TB models within the gradient approximation for the matrix elements of the linear momentum. The selection rules for allowed dipole transitions were first discussed by Ajiki and Ando [10] in the study of the low-energy optical absorption due to interband transitions as a probe of the Aharonov–Bohm effect. π-TB calculations of the plasmons and optical properties of carbon nanotube systems were presented by two groups [11, 12]. The polarized optical conductivity was calculated for a number of nanotubes with radii between 4 and 8 Å within an all-valence TB model [13]

based on a symmetry-adapted scheme which is essentially the one introduced in [5]. *Ab initio* calculations of the dielectric function were carried out for a (5, 7) nanotube [14] and for three small-radius nanotubes: (3, 3), (5, 0) and (4, 2) [15, 16]. Among the various computed quantities, the optical transition energies are of great importance for the nanotube characterization since they can be of help for the assignment of the optical absorption spectra of nanotube samples. The predictions of the π-TB models have been widely used for these purposes [17]. However, the π-TB models cannot reproduce satisfactorily the electronic structure and optical properties of small-radius nanotubes. Recently, a π-TB model with a chirality- and diameter-dependent nearest-neighbour hopping integral was used to relate well-resolved features in the UV–VIS–NIR spectra of individual nanotubes to electronic excitations in specific tube types [18]. The precise computation of the optical properties of nanotubes requires the implementation of more realistic approaches. The *ab initio* calculations are hindered by the large number of atoms in the unit cell of most nanotubes. An alternative approach can be to use a well-tuned non-orthogonal TB model (see e.g. [3]–[5, 13, 19]) based on a symmetry-adapted scheme that will allow one to handle nanotubes with a large number of carbon atoms in the unit cell (see e.g. [5, 13, 20, 21]).

Here, results of structural optimization and calculation of the electronic band structure and dielectric function of a large number of nanotubes, carried out within a symmetry-adapted non-orthogonal tight-binding model, are presented. First, the main relations between the structural parameters of nanotubes are introduced in section 2. The symmetry-adapted non-orthogonal tight-binding model is presented in section 3. The optimized nanotube structure of all nanotubes, the obtained electronic band structure and the dielectric function for three small-radius nanotubes, as well as the transition energies for all armchair and zigzag nanotubes are given in section 4. The conclusions are presented in section 5.

2. The nanotube structure

The ideal single-walled carbon nanotube can be viewed as obtained by the rolling up of an infinite strip of a graphene sheet into a seamless cylinder [3]–[5]. The seamlessness of the tube means coincidence of lattice points connected on the sheet by a lattice vector $L_1\boldsymbol{a}_1 + L_2\boldsymbol{a}_2$ ($\boldsymbol{a}_1$ and $\boldsymbol{a}_2$ are the primitive translation vectors of the sheet, L_1 and L_2 are integer numbers, $L_1 \geqslant L_2 \geqslant 0$). This ideal nanotube can be specified uniquely by the pair of indices (L_1, L_2). We recall that a two-atom unit cell can be mapped onto the entire graphene sheet by the use of two primitive translation vectors. Similarly, a two-atom unit cell can be mapped onto the entire tube by use of two different screw operators (see figure 1) [6]. By definition, a screw operator $\{S_i \,|\, \boldsymbol{t}_i\}$ ($i = 1, 2$) executes a rotation of the position vector of an atom at an angle φ_i about the tube axis with a rotation matrix S_i and a translation of the position vector at a vector $\boldsymbol{t}_i$ along the tube axis. Thus the equilibrium position vector $\boldsymbol{x}(\boldsymbol{l}k)$ of the kth atom in the $\boldsymbol{l}$th cell ($\boldsymbol{l} = (l_1, l_2)$) can be obtained from the position vectors of the atoms in the zeroth unit cell $\boldsymbol{x}(k) \equiv \boldsymbol{x}(\boldsymbol{0}k)$ ($k = 1, 2$) as

$$\boldsymbol{x}(\boldsymbol{l}k) = \{S_1 \,|\, \boldsymbol{t}_1\}^{l_1}\{S_2 \,|\, \boldsymbol{t}_2\}^{l_2}\boldsymbol{x}(k) = S_1^{l_1}S_2^{l_2}\boldsymbol{x}(k) + l_1\boldsymbol{t}_1 + l_2\boldsymbol{t}_2. \tag{1}$$

We adopt the abbreviated notation $S_1(\boldsymbol{l}) = S_1^{l_1}S_2^{l_2}$ and $\boldsymbol{t}(\boldsymbol{l}) = l_1\boldsymbol{t}_1 + l_2\boldsymbol{t}_2$ and rewrite equation (1) in the form

$$\boldsymbol{x}(\boldsymbol{l}k) = \{S(\boldsymbol{l}) \,|\, \boldsymbol{t}(\boldsymbol{l})\}\boldsymbol{x}(k) = S(\boldsymbol{l})\boldsymbol{x}(k) + \boldsymbol{t}(\boldsymbol{l}). \tag{2}$$

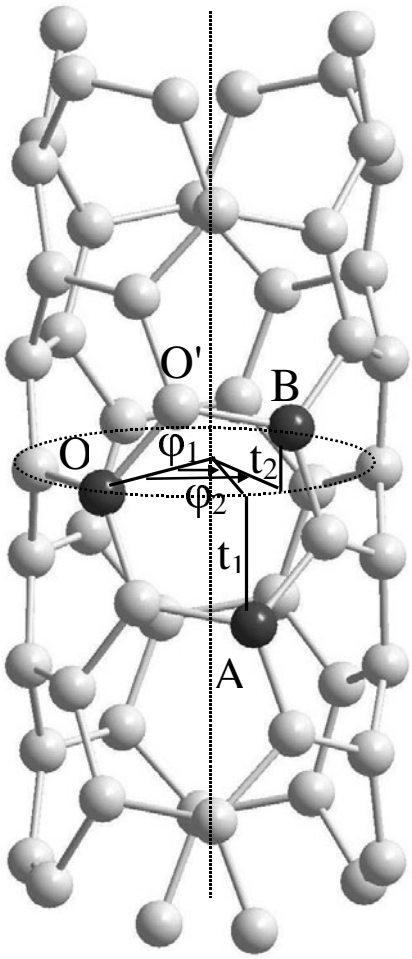

Figure 1. Illustration of the two different screw operations that can be used to map a pair of atoms O and O′ onto the entire tube. The screw operations bring to coincidence atom O with atom A (or B) on rotation at an angle φ_1 (or φ_2) around the tube axis and translation at a distance t_1 (or t_2).

In a similar way, one of the atoms in the two-atom unit cell can be mapped unto the other atom by use of a screw operation defined by an angle φ' and a translation vector $\boldsymbol{t}'$.

The primitive rotation angles and the primitive translations of the two types of screw operations can be found from the translational periodicity and rotational boundary conditions

$$N_1\varphi_1 + N_2\varphi_2 = 0, \tag{3}$$

$$L_1\varphi_1 + L_2\varphi_2 = 2\pi, \tag{4}$$

$$N_1\boldsymbol{t}_1 + N_2\boldsymbol{t}_2 = \boldsymbol{T}, \tag{5}$$

$$L_1\boldsymbol{t}_1 + L_2\boldsymbol{t}_2 = \boldsymbol{0}. \tag{6}$$

Here $\boldsymbol{T}$ is the primitive translation vector of the nanotube. N_1 and N_2 are integer numbers defining $\boldsymbol{T}$ on the graphene sheet and are given by the relations

$$N_1 = (L_1 + 2L_2)/d, \tag{7}$$

$$N_2 = -(2L_1 + L_2)/d. \tag{8}$$

The integer number d is equal to the highest common divisor d' of L_1 and L_2 if $L_1 - L_2$ is not a multiple of $3d'$ or d is equal to $3d'$ if $L_1 - L_2$ is a multiple of $3d'$. Using equations (3)–(6), one obtains

$$\varphi_1 = 2\pi N_2/N_c, \tag{9}$$

$$\varphi_2 = -2\pi N_1/N_c, \tag{10}$$

$$\boldsymbol{t}_1 = (L_2/N_c)\boldsymbol{T}, \tag{11}$$

$$\boldsymbol{t}_2 = -(L_1/N_c)\boldsymbol{T}. \tag{12}$$

Here, the total number of atomic pairs in the unit cell, N_c, is given by

$$N_c = N_1L_2 - N_2L_1 = 2(L_1^2 + L_1L_2 + L_2^2)/d. \tag{13}$$

The position vectors of the atoms of the tube can be written as $\boldsymbol{x}(nlk) = \boldsymbol{x}(lk) + n\boldsymbol{T}$, where the integer number n labels the translational unit cells and $\boldsymbol{l}$ labels the two-atom unit cells in each translational unit cell.

A nanotube can be characterized alternatively by its radius R and chiral angle (or wrapping angle) θ which is the angle between the tube circumference and the nearest zigzag of C–C bonds, $0^\circ \leqslant \theta < 30^\circ$ [3]. For the 'rolled-up' structure these quantities are given by

$$R = \sqrt{3(L_1^2 + L_1L_2 + L_2^2)}a_{C\text{–}C}/2\pi, \tag{14}$$

$$T = 2\sqrt{3}\pi R/d, \tag{15}$$

$$\theta = \tan^{-1}(\sqrt{3}L_2/(L_2 + 2L_1)), \tag{16}$$

where $a_{C\text{–}C}$ is the C–C bond length in graphene. The 'rolled-up' structure is useful when the nanotube structure cannot be optimized, as is the case with some tight-binding models using fixed parameters. However, in other tight-binding models with explicit dependence of the parameters on the interatomic separations and in all *ab initio* models of the electronic structure one should optimize the nanotube structure. In the simplest case, only the bond lengths and valence angles for the two atoms in the two-atom unit cell are varied in the optimization procedure preserving the translational and the screw symmetry of the tube. Thus, R, T, φ', and t' can be considered as independent structural parameters. For the optimized structure the above relations between R, T and θ, and L_1, L_2 will generally no longer hold. It is worth noting that, if the translational symmetry condition is not imposed, the chiral tubes can loose their translational symmetry upon optimization. The error due to imposing this condition (see equation (28)) is expected to be small because of the usually large number of atoms in the unit cell of most chiral tubes.

3. The symmetry-adapted non-orthogonal tight-binding model

The electronic band structure of a periodic structure is usually obtained by solving the one-electron Schrödinger equation

$$\left[-\frac{\hbar^2\nabla^2}{2m} + V(\boldsymbol{r})\right]\psi_{\boldsymbol{k}}(r) = E_{\boldsymbol{k}}\psi_{\boldsymbol{k}}(r), \tag{17}$$

where m is the electron mass, $V(\boldsymbol{r})$ the effective periodic potential, $\psi_{\boldsymbol{k}}(\boldsymbol{r})$ and $E_{\boldsymbol{k}}$ are the one-electron wavefunction and energy depending on the wavevector $\boldsymbol{k}$. This equation can be solved by representing $\psi_{\boldsymbol{k}}(\boldsymbol{r})$ as a linear combination of basis functions $\varphi_{\boldsymbol{k}r}(\boldsymbol{r})$

$$\psi_{\boldsymbol{k}}(\boldsymbol{r}) = \sum_r c_{\boldsymbol{k}r}\varphi_{\boldsymbol{k}r}(\boldsymbol{r}). \tag{18}$$

In the tight-binding approach, the φs are constructed from atomic orbitals centred at the atoms. Let us denote by $\chi_r(\boldsymbol{R}(\boldsymbol{l}) - \boldsymbol{r})$ the rth atomic orbital centred at an atom with position vector $\boldsymbol{R}(\boldsymbol{l})$ in the $\boldsymbol{l}$th unit cell. Bloch's condition for the basis functions φ is satisfied for the following linear combination of χs:

$$\varphi_{\boldsymbol{k}r}(\boldsymbol{r}) = \frac{1}{\sqrt{N}}\sum_{\boldsymbol{l}} \mathrm{e}^{\mathrm{i}\boldsymbol{k}\cdot\boldsymbol{R}(\boldsymbol{l})}\chi_r(\boldsymbol{R}(\boldsymbol{l}) - \boldsymbol{r}), \tag{19}$$

where N is the number of unit cells in the system. In the case of graphene, the lattice parameters are equal ($a = b$) and therefore $\boldsymbol{R}(\boldsymbol{l}) = l_1\boldsymbol{a}_1 + l_2\boldsymbol{a}_2 = \boldsymbol{l}a$. Then, one can introduce a dimensionless wavevector $\boldsymbol{k} = (k_1, k_2)$ and rewrite equation (19) as

$$\varphi_{\boldsymbol{k}r}(\boldsymbol{r}) = \frac{1}{\sqrt{N}}\sum_{\boldsymbol{l}} \mathrm{e}^{\mathrm{i}\boldsymbol{k}\cdot\boldsymbol{l}}\chi_r(\boldsymbol{R}(\boldsymbol{l}) - \boldsymbol{r}). \tag{20}$$

After substitution of equation (20) in equation (17), the electronic problem for graphene is transformed into a matrix eigenvalue problem.

In the case of nanotubes, one can still use the equations above. However, the number of atoms in the unit cell of some nanotubes can be very large, leading to a large-size matrix equation for the electronic problem. We notice, however, that any nanotube has a screw symmetry, which allows one to use only a two-atom unit cell for the electronic problem [6]. To implement explicitly the screw symmetry, we start with symmetrized wavefunctions, which satisfy a modified Bloch's condition under screw operations with any $\boldsymbol{l}$. Wavefunctions with such a property have the form

$$\varphi_{\boldsymbol{k}r}(\boldsymbol{r}) = \frac{1}{\sqrt{N}}\sum_{\boldsymbol{l}r'} \mathrm{e}^{\mathrm{i}\boldsymbol{k}\cdot\boldsymbol{l}}T_{rr'}(\boldsymbol{l})\chi_{r'}(\boldsymbol{R}(\boldsymbol{l}) - \boldsymbol{r}), \tag{21}$$

where $\boldsymbol{k} = (k_1, k_2)$ is an yet undefined two-component wavevector of the nanotube and $T_{rr'}(\boldsymbol{l})$ are appropriate rotation matrices rotating a given atomic-type orbital to the same orientation with respect to the nanotube surface for all atoms. It is straightforward to verify that a screw operation transforms a symmetrized wavefunction into itself up to a Bloch exponent.

Substituting equation (21) in equation (17), we obtain

$$\sum_{r'} c_{\boldsymbol{k}r'} H_{\boldsymbol{k}rr'} = E_{\boldsymbol{k}} \sum_{r'} c_{\boldsymbol{k}r'} S_{\boldsymbol{k}rr'}, \tag{22}$$

where

$$H_{\boldsymbol{k}rr'} = \sum_{\boldsymbol{l}r''} \mathrm{e}^{\mathrm{i}\boldsymbol{k}\cdot\boldsymbol{l}} H_{rr''}(\boldsymbol{l}) T_{r''r'}(\boldsymbol{l}), \tag{23}$$

$$S_{\boldsymbol{k}rr'} = \sum_{\boldsymbol{l}r''} \mathrm{e}^{\mathrm{i}\boldsymbol{k}\cdot\boldsymbol{l}} S_{rr''}(\boldsymbol{l}) T_{r''r'}(\boldsymbol{l}), \tag{24}$$

and

$$H_{rr'}(\boldsymbol{l}) = \int \mathrm{d}\boldsymbol{r}\, \chi_r(\boldsymbol{R}(\boldsymbol{0}) - \boldsymbol{r}) \hat{H} \chi_{r'}(\boldsymbol{R}'(\boldsymbol{l}) - \boldsymbol{r}), \tag{25}$$

$$S_{rr'}(\boldsymbol{l}) = \int \mathrm{d}\boldsymbol{r}\, \chi_r(\boldsymbol{R}(\boldsymbol{0}) - \boldsymbol{r}) \chi_{r'}(\boldsymbol{R}'(\boldsymbol{l}) - \boldsymbol{r}). \tag{26}$$

The quantities $H_{rr'}(\boldsymbol{l})$ and $S_{rr'}(\boldsymbol{l})$ are the matrix elements of the Hamiltonian $\hat{H}$ and the overlap matrix elements, respectively. The vectors $\boldsymbol{R}(\boldsymbol{l})$ and $\boldsymbol{R}'(\boldsymbol{l})$ are position vectors of atoms in the $\boldsymbol{l}$th two-atom unit cell.

The wavevector components k_1 and k_2 can be determined by imposing the rotational boundary and translational periodicity conditions which yields the relations

$$k_1 L_1 + k_2 L_2 = 2\pi l, \tag{27}$$

$$k_1 N_1 + k_2 N_2 = k, \tag{28}$$

where k is the one-dimensional wavevector of the tube ($-\pi \leqslant k \leqslant \pi$) and the integer number l labels the electronic energy levels with a given k ($l = 0, 1, \ldots, N_c - 1$). From equations (27) and (28) we obtain k_1 and k_2

$$k_1 = (2\pi N_2 l - L_2 k)/N_c, \tag{29}$$

$$k_2 = (L_1 k - 2\pi N_1 l)/N_c. \tag{30}$$

The substitution of equations (29) and (30) into equations (21)–(24) yields

$$\varphi_{klr}(\boldsymbol{r}) = \frac{1}{\sqrt{N}} \sum_{\boldsymbol{l}} \mathrm{e}^{\mathrm{i}(\alpha(\boldsymbol{l})l + z(\boldsymbol{l})k)} T_{rr'} \chi_{r'}(\boldsymbol{R}(\boldsymbol{l}) - \boldsymbol{r}), \tag{31}$$

$$\sum_{r'} c_{klr'} H_{klrr'} = E_{kl} \sum_{r'} c_{klr'} S_{klrr'}, \tag{32}$$

$$H_{klrr'} = \sum_{\boldsymbol{l}r''} \mathrm{e}^{\mathrm{i}(\alpha(\boldsymbol{l})l + z(\boldsymbol{l})k)} H_{rr''}(\boldsymbol{l}) T_{r''r'}(\boldsymbol{l}), \tag{33}$$

$$S_{klrr'} = \sum_{\boldsymbol{l}r''} \mathrm{e}^{\mathrm{i}(\alpha(\boldsymbol{l})l + z(\boldsymbol{l})k)} S_{rr''}(\boldsymbol{l}) T_{r''r'}(\boldsymbol{l}), \tag{34}$$

where $\boldsymbol{l}$ runs over the indices of the two-atom unit cells in the translational unit cell. The quantities $\alpha(\boldsymbol{l})$ and $z(\boldsymbol{l})$ are given by

$$\alpha(\boldsymbol{l}) = 2\pi(l_1 N_2 - l_2 N_1)/N_c, \tag{35}$$

$$z(\boldsymbol{l}) = (L_1 l_2 - L_2 l_1)/N_c. \tag{36}$$

The set of linear algebraic equations (32) has non-trivial solutions for the coefficients c only for energies E which satisfy the characteristic equation

$$\| H_{klrr'} - E_{kl} S_{klrr'} \| = 0. \tag{37}$$

The solutions of equation (37), E_{klm}, are the electronic energy levels; the energy bands are labelled by the composite index lm ($m = 1, 2, \ldots$). The corresponding eigenvectors c_{klmr} are determined from equation (32).

The symmetry-adapted approach to the calculation of the electronic band structure of nanotubes has the important advantage of a large reduction in the computational time. Indeed, the calculation of the band energies for a given k needs time scaling as the cube of the size of the two-atom eigenvalue problem (8^3 for 4 electrons per carbon atom) times the number of two-atom unit cells N_c. On the other hand, a straightforward calculation of the same band energies will require time scaling as the cube of the size of the $2N_c$-atom eigenvalue problem, i.e. $(8N_c)^3$. The presented symmetry-adapted approach has been applied to the vibrational eigenvalue problem [20, 21] and can be used in the calculation of any property of a nanotube within a microscopic model.

The total energy of a nanotube (per unit cell) is given by

$$E = \sum_{klm}^{occ} E_{klm} + \frac{1}{2} \sum_i \sum_j \phi(r_{ij}), \tag{38}$$

where the first term is the band energy (the summation is over all occupied states) and the second term is the repulsive energy, consisting of repulsive pair potentials $\phi(r)$ between pairs of nearest neighbours. The increase of the total energy (per carbon atom) when a graphene strip is folded into a nanotube is the strain (or folding) energy E_{st}:

$$E_{st} = E/(2N_c) - E_{Gr}/2, \tag{39}$$

where E_{Gr} is the total energy of graphene per unit cell.

For the structural optimization of a nanotube one needs the band and the repulsive contributions to the forces acting on the atoms. The band contribution to the force in α direction on the atom with a position vector $\boldsymbol{R}(\boldsymbol{0})$ is given by the Hellmann–Feynman theorem

$$F_\alpha = \sum_{klm}^{occ} \frac{\partial E_{klm}}{\partial R_\alpha(\boldsymbol{0})} = \sum_{klm}^{occ} \sum_{rr'} c^*_{klmr} \frac{\partial (H_{klrr'} - E_{klm} S_{klrr'})}{\partial R_\alpha(\boldsymbol{0})} c_{klmr'}. \tag{40}$$

The repulsive contribution is the first derivative of the total repulsive energy with respect to the position vector $\boldsymbol{R}(\boldsymbol{0})$.

The imaginary part of the dielectric function in the random-phase approximation is given by [22]

$$\varepsilon_2(\omega) = \frac{4\pi^2 e^2}{m^2\omega^2} \sum_{l'clv} \frac{2}{2\pi} \int \mathrm{d}k |p_{kl'cklv,\mu}|^2 \delta(E_{kl'c} - E_{klv} - \hbar\omega), \tag{41}$$

where $\hbar\omega$ is the photon energy, e the elementary charge and m the electron mass. The sum is over all occupied (v) and unoccupied (c) states. $p_{kl'cklv,\mu}$ is the matrix element of the component of the momentum operator in the direction μ of the light polarization

$$p_{kl'cklv,\mu} = \int \mathrm{d}\boldsymbol{r}\, \psi^*_{kl'c}(\boldsymbol{r})\, \hat{p}_\mu \psi_{klv}(\boldsymbol{r}). \tag{42}$$

Substituting the one-electron wavefunctions given by equations (18) and (31) in equation (42), one obtains the non-zero matrix elements

$$p_{kl'cklv,\mu} = f_{ll'\mu} \sum_{rr'} c^*_{kl'cr'} c_{klvr} \sum_{lr''} \mathrm{e}^{-\mathrm{i}(\alpha(\boldsymbol{l})l + z(\boldsymbol{l})k)}\, p_{r'r'',\mu}(\boldsymbol{l}) T_{rr''}(\boldsymbol{l}), \tag{43}$$

where

$$p_{rr',\mu}(\boldsymbol{l}) = \int \mathrm{d}\boldsymbol{r}\, \chi_r(\boldsymbol{R}(\boldsymbol{0}) - \boldsymbol{r})\, \hat{p}_\mu \chi_{r'}(\boldsymbol{R}'(\boldsymbol{l}) - \boldsymbol{r}). \tag{44}$$

For z-axis along the tube axis, the quantities $f_{ll',\mu}$ are given by

$$f_{ll'x} = f_{ll',y} = (\delta_{l',l+1} + \delta_{l',l-1})/2, \tag{45}$$

$$f_{ll',z} = \delta_{ll'}. \tag{46}$$

Equations (45) and (46) express the selection rules for allowed dipole optical transitions, namely, optical transitions are only allowed between states with the same l for parallel polarization and between states with l and l' differing by 1 for perpendicular polarization (compare with [10]). Further on, from Maxwell's relation $\varepsilon = \tilde{n}^2$ ($\tilde{n}$ is the complex refractive index), the refractive index $n = \mathrm{Re}\,\tilde{n}$ and the extinction coefficient $\kappa = \mathrm{Im}\,\tilde{n}$ are readily obtained. The relations $\alpha = 2\omega\kappa/c$ (c is the light velocity in vacuum) and $R = |(\tilde{n} - 1)/(\tilde{n} + 1)|^2$ allow one to derive the absorption coefficient α and the reflection coefficient for normal incidence R.

Let us consider a single pair of valence and conduction bands with maximum and minimum separated by a direct gap E_{cv} corresponding to an allowed optical transition $v \to c$. Assuming that the matrix elements $p_{cv,\mu}$ are independent of k, it is straightforward to show that the contribution to ε_2 from these bands is given by

$$\varepsilon_2 = \frac{2\pi e^2}{m^2\omega^2} \sqrt{\frac{2m^*_{cv}}{\hbar^2}} |p_{cv,\mu}|^2 \frac{1}{\sqrt{\hbar\omega - E_{cv}}}. \tag{47}$$

Here m^* is the reduced effective mass for the two bands. Alternatively, for a pair of valence and conduction bands with minimum and maximum separated by energy E_{cv} one obtains

$$\varepsilon_2 = \frac{2\pi e^2}{m^2\omega^2}\sqrt{\frac{2m^*_{cv}}{\hbar^2}}|p_{cv,\mu}|^2\frac{1}{\sqrt{E_{cv}-\hbar\omega}}. \tag{48}$$

In the general case, the graph $\varepsilon_2(\omega)$ will consist of two types of spikes close in form to those described by equations (47) and (48). From the derivation of the latter two equations it is clear that the electron density of states (DOS) versus ω will have the same two types of spikes.

4. Results and discussion

The parameters of the non-orthogonal tight-binding (nTB) model are taken from a density-functional-based study [23]. In the case of graphite, these parameters showed excellent performance in the calculation of the equilibrium lattice parameter and the cohesive energy. The tight-binding electronic structure of graphene corresponds well to the *ab initio* results for the valence and conduction bands in the energy region (–3, 3) eV (the Fermi energy is set to zero). The calculated energy separation between the π and π^* bands at the M point of the Brillouin zone of graphene was 4.9 eV which agrees with the *ab initio* LDA result of ∼4.4 eV [16] while the π-TB value was ∼5.9 eV [4]. This implies that the optical properties of graphene should be reproduced with the same accuracy up to ∼6 eV. The same reliability region should be valid for carbon nanotubes as well.

Here, the structure of 187 nanotubes with radii R in the range from 2 to 15 Å and $N_c < 400$ is optimized within the nTB model. The optimization is carried out under the constraint that all atoms lie on a cylindrical surface and R, T, φ' and t' are considered as independent structural parameters. The total energy and the forces on the atoms of the two-atom unit cell are calculated with a tube-dependent number of k points N_k for which these quantities converge. For example, $N_k = 60$ for the tube (3, 3) and $N_k = 30$ for the tube (9, 9). It was found that N_k decreases nearly proportionally to $1/N_c$. It is clearly seen in figure 2 that, upon optimization, the nanotubes widen laterally and shorten in length, which has as a consequence a decrease of the chiral angle. This effect depends on the nanotube chirality. Armchair tubes have the smallest increase in radius and almost zero shortening and largest decrease in the chiral angle. Zigzag nanotubes have largest increase in the radius and medium shortening (the chiral angle is zero by definition). Chiral nanotubes have a moderate increase in the radius, largest shortening and medium decrease of the chiral angle. The trend of change of the structural parameters corresponds to the *ab initio* results for several nanotubes in [16, 24, 25]. For example, we obtain an increase in the radius for tubes (4, 4) and (10, 10) of 1.6 and 0.3% compared to 1.2 and 0.2% [24]. For tubes (5, 0), (3, 3) and (4, 2) with non-optimized radii of 1.96, 2.03 and 2.07 Å, we obtain optimized radii of 2.05, 2.12 and 2.14 Å that are in fair agreement with the *ab initio* results 2.04, 2.10 and 2.14 Å [16], and 2.06, 2.12 and 2.17 [25]. The maximum values of the changes in R, θ and T are 0.1 Å, 1°, 0.4 Å, and the relative changes are 5, 4 and 1%, respectively. The optimized nanotube structure is characterized with non-equal bond lengths and bond angles for atoms in the two-atom unit cell. The differences between the optimized and non-optimized structures decrease with the increase in radius and can be ignored for radii larger than about 5 Å. It is interesting to compare the strain energy calculated in the present model (figure 3) with the *ab initio* results [24]–[27]. Fitting the strain energy versus radius with $E_{st} = C/R^2$ [28] we obtain $C = 2.133\,\text{eV}\,\text{Å}^2$ per atom which

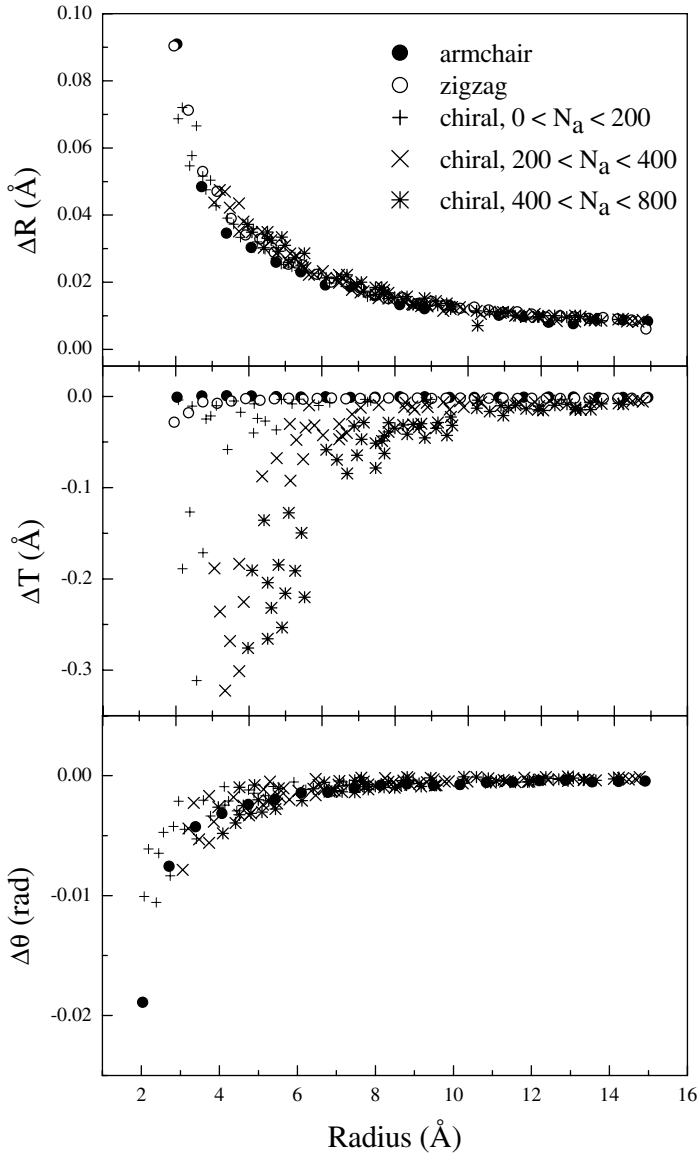

Figure 2. Absolute changes of the radius R, chiral angle θ and primitive translation T for all nanotubes with radii between 2 and 15 Å and $N_c < 400$ upon optimization. It is clearly seen that the nanotubes widen laterally, shorten in length and the chiral angle decreases.

agrees well with 2.20 eV Å^2 per atom (tubes (3, 3) to (9, 9)) [26], 2.00 eV Å^2 per atom (tubes (8, 8) to (12, 12)) [27], 2.00 eV Å^2 per atom (tubes (4, 4) to (10, 10)) [24], 2.05 eV Å^2 per atom (tubes (4, 4) to (10, 10), (10, 0), (8, 4)) [24], 2.1 eV Å^2 per atom (ten tubes with 1.7 Å $< R <$ 2.5 Å) [25].

The calculated electronic band structure of three small-radius nanotubes (5, 0), (3, 3) and (4, 2) within the nTB and π-TB models is shown in figure 4. It is seen that the nTB band structure of these tubes deviates considerably from the π-TB one. Similar to the *ab initio* band structure [15, 16], the large curvature of these tubes leads to large σ^*–π^* rehybridization which modifies the nTB band structure with respect to that of π-TB [7, 15, 16]. In particular, nanotube (5, 0) is metallic contrary to the predictions of π-TB. The crossing of the bands at the

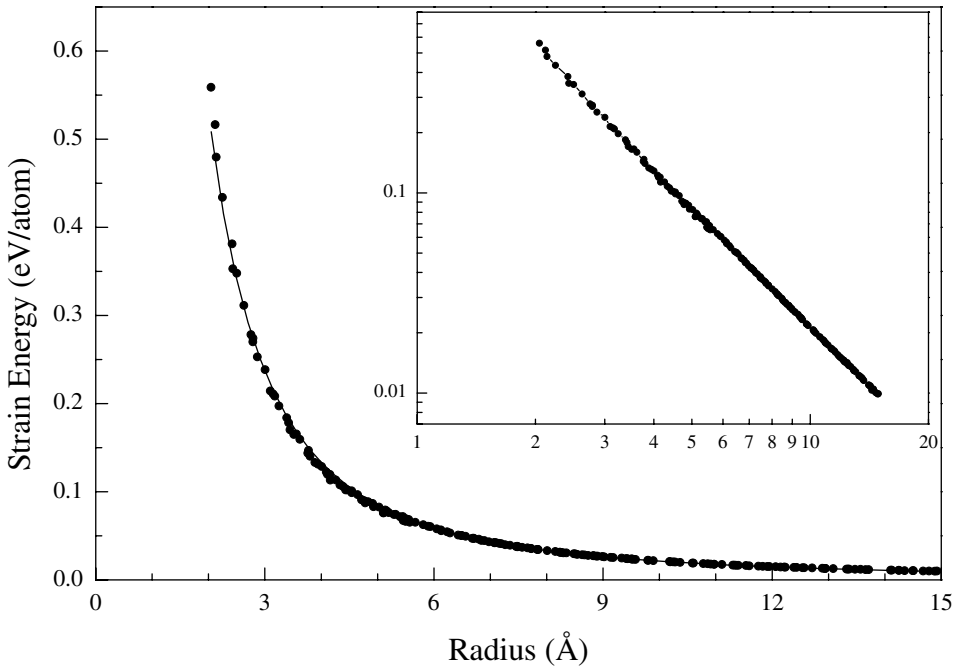

Figure 3. Calculated strain energy of all nanotubes as in figure 2. The line is the best fit of the obtained points with a power law C/R^2. The inset shows the same points in a log–log scale.

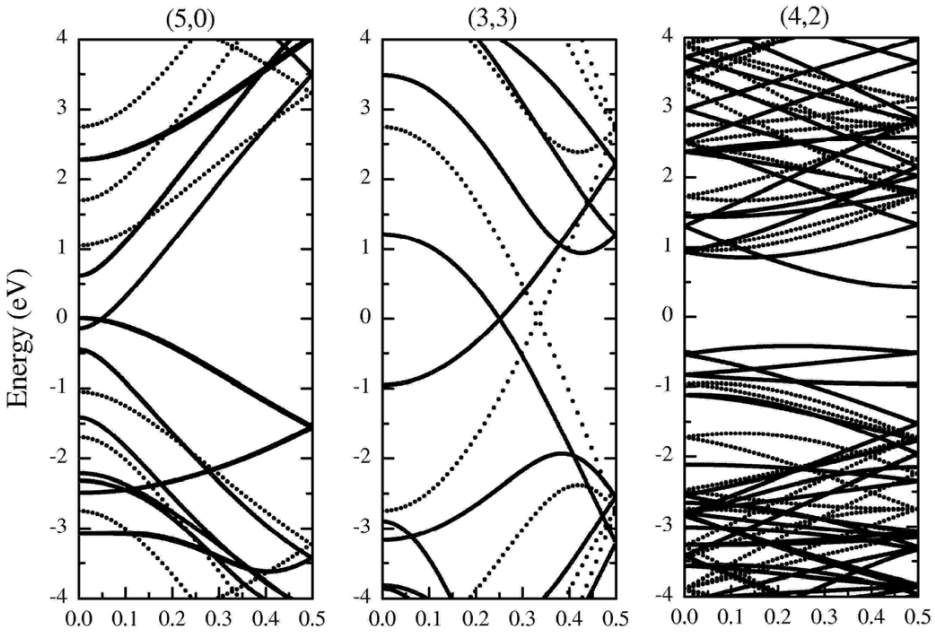

Figure 4. Calculated electronic band structure of nanotubes (5, 0), (3, 3) and (4, 2) in the energy range between -4 and 4 eV with respect to the Fermi energy. Dotted lines are results from the π-TB model with transfer integral $\gamma_0 = 2.75$ eV.

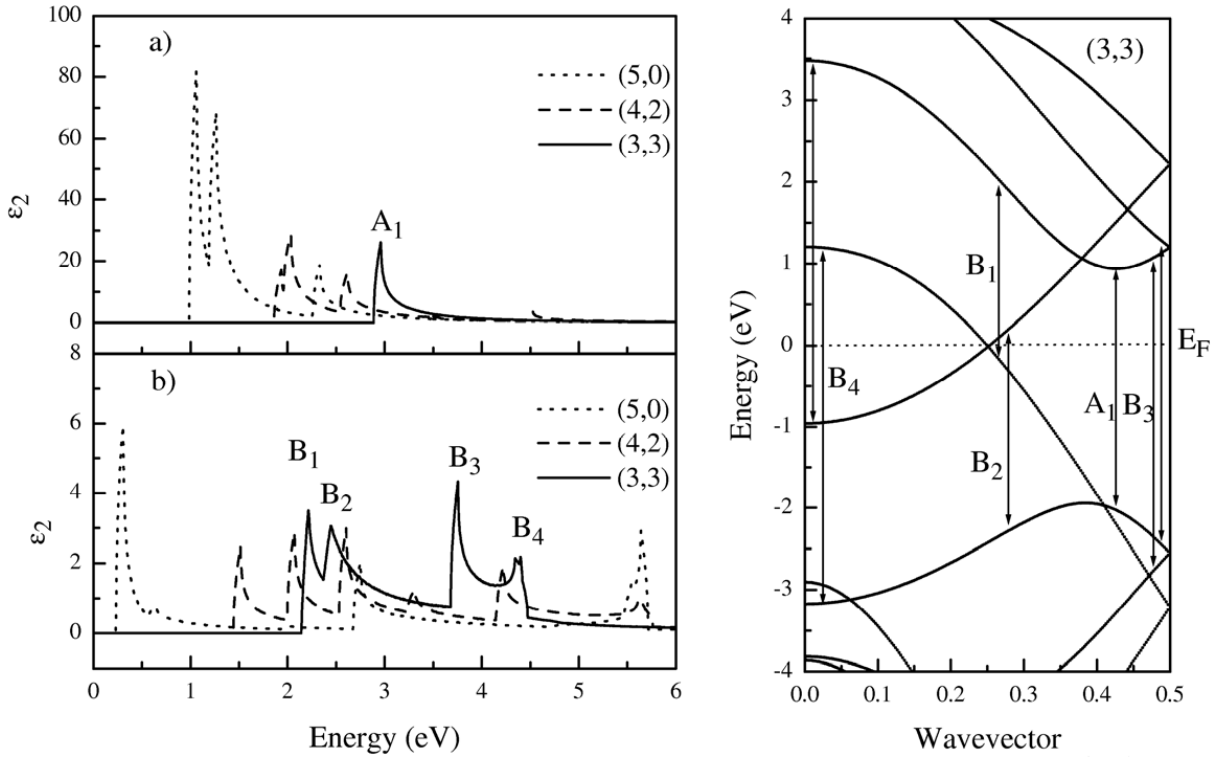

Figure 5. Left: calculated dielectric function ε_2 of nanotubes (5, 0) (dotted line), (4, 2) (dashed line) and (3, 3) (solid line), for parallel polarization (upper panel) and perpendicular polarization (lower panel) in the energy range from 0 to 6 eV. Right: electronic band structure of nanotube (3, 3) close to the Fermi energy E_F. The arrows indicate the optical transitions giving rise to peaks of ε_2.

Fermi level in nanotube (3, 3) is at $k \approx 0.25\pi$ instead of at $k = (2/3)\pi$. Nanotube (4, 2) has an indirect band gap of ≈0.83 eV which is twice as small as the direct gap of the π-TB model but is a little larger than the *ab initio* value [15, 16].

The calculated imaginary part of the dielectric function of nanotubes (5, 0), (3, 3) and (4, 2) within the nTB model for parallel and perpendicular polarization in the energy range from 0 to 6 eV is shown in figure 5. The form of the peaks follows approximately equations (47) and (48). The peaks in the spectra for parallel polarization originate from minima and maxima of occupied and unoccupied bands with the same quantum number l. For example, peak A_1 in figure 5 can be associated with an optical transition between a maximum of an occupied band of ~ -2 eV and a minimum of an unoccupied band of ∼1 eV of tube (3, 3). These minima and maxima give rise to spikes in the electronic density of states of the nanotubes. The peaks in the spectra for perpendicular polarization originate from minima and maxima of occupied and unoccupied bands as well as from states on parallel parts of occupied and unoccupied bands with quantum numbers l and $l \pm 1$. For example, peaks B_1 and B_2 come from such transitions near the crossing point of the bands at the Fermi level; peak B_3 comes from states near the Brillouin zone boundary; peak B_4 is due to transitions between minima and maxima of bands at the zone centre. The calculated transition energies for the three tubes (5, 0) (1.0, 1.2 eV), (3, 3) (2.9 eV), and (4, 2) (1.85, 1.96 eV) correspond well to the *ab initio* results 1.2, 2.9 and

1.9 eV [16]. This is an indirect evidence for the applicability of the used density-functional-theory-based non-orthogonal tight-binding model to the optical properties of carbon nanotubes. It should be noted that the depolarization effects are not accounted for in the calculation of ε_2 for perpendicular polarization. On the other hand, the small lateral size of the nanotubes can lead to strong depolarization effects and to significant reduction of the dielectric function [10]. The precise inclusion of the depolarization effects is expected to result in corrections to the calculated dielectric function for perpendicular polarization mainly in the peak height. The importance of the knowledge of the dielectric function for both parallel and perpendicular polarizations has been underlined recently in a cross-polarized resonant-Raman study of nanotubes [29].

The electronic band structure and the imaginary part of the dielectric function for parallel light polarization are calculated within the nTB model for a large number of small-radius nanotubes. These quantities can be illustrated by means of the band gap and the optical transition energies. The band gaps are equal to the lowest transition energies for parallel polarization of almost all semiconducting tubes. Exceptions are some very-small-radius tubes where the rehybridization effects lead to indirect band gaps (e.g. tubes (4, 2), (5, 1), etc.). The nTB band gaps for the non-optimized (nTB1) and optimized (nTB2) structures of all zigzag tubes with $2\,\text{Å} < R < 15\,\text{Å}$ are given in figure 6 and are compared with π-TB results. First of all, small band gaps appear in all zigzag tubes that are predicted to be metallic by the π-TB model. It is seen in figure 6 that, in the case of zigzag tubes $(6 + 3n, 0)$, the curvature-induced gaps for the optimized structure are larger than for the non-optimized one. The band gaps derived here for optimized zigzag tubes (6, 0), (9, 0), (12, 0) and (15, 0) are 0.45, 0.127, 0.046 and 0.025 eV respectively. For comparison, the results for the gaps of all-valence TB models with parameters fitted to experimental data are 0.20 and 0.04 [3], 0.05 and 0.07 eV [7] for tubes (6, 0) and (9, 0); 0.18 and 0.08 for tubes (6, 0) and (9, 0) [19]. The LDA gaps are (tube (6, 0) is found to be metallic): 0.17 eV for tube (9, 0) [7], 0.093, 0.078 and 0.028 eV for tubes (9, 0), (12, 0) and (15, 0) [30]. The gaps measured by scanning tunnelling spectroscopy for tubes (9, 0), (12, 0) and (15, 0) are 0.080, 0.042 and 0.029 eV [31]. It is clear that the gaps calculated here correspond well to the LDA and the experimental values, together with those of other TB models. The band gaps of semiconducting zigzag tubes $(5 + 3n, 0)$ and $(7 + 3n, 0)$ are smaller than those of the π-TB model. Upon optimization within the nTB model, the band gaps are modified and the changes being largest $\approx$0.5 eV in the limit of very small radii. Therefore, although the effect of structural optimization is smaller than that of σ^*–π^* rehybridization, the former is not always negligible and structural optimization is necessary for higher reliability of the derived optical transition energies.

Finally, the optical transition energies for all 101 nanotubes with $2\,\text{Å} < R < 8\,\text{Å}$ and $N_c < 400$ are derived from the dielectric function calculated for the optimized nanotube structure within the nTB model. It is clear from figure 7, where the transition energies are presented in comparison with the energies of the π-TB model, that the predictions of these two models deviate significantly for small tube radii. It is seen that the curvature-induced rehybridization effects are largest for small radii and decrease with increase in tube radius. For very small radii of $\approx$2 Å, the π-TB results overestimate the nTB transition energies up to $\approx$0.5 eV. For moderate radii, the π-TB results are upshifted by about $\approx$0.1 eV. By *ab initio* LDA calculations similar shifts of $\approx$0.1 eV were obtained for nanotubes with radii in the range $5\,\text{Å} < R < 7.5\,\text{Å}$ [9]. The transition energies determine the conditions for resonant Raman scattering in nanotubes. Most of the characterizations by Raman scattering have been based on the use of the predictions of a π-TB

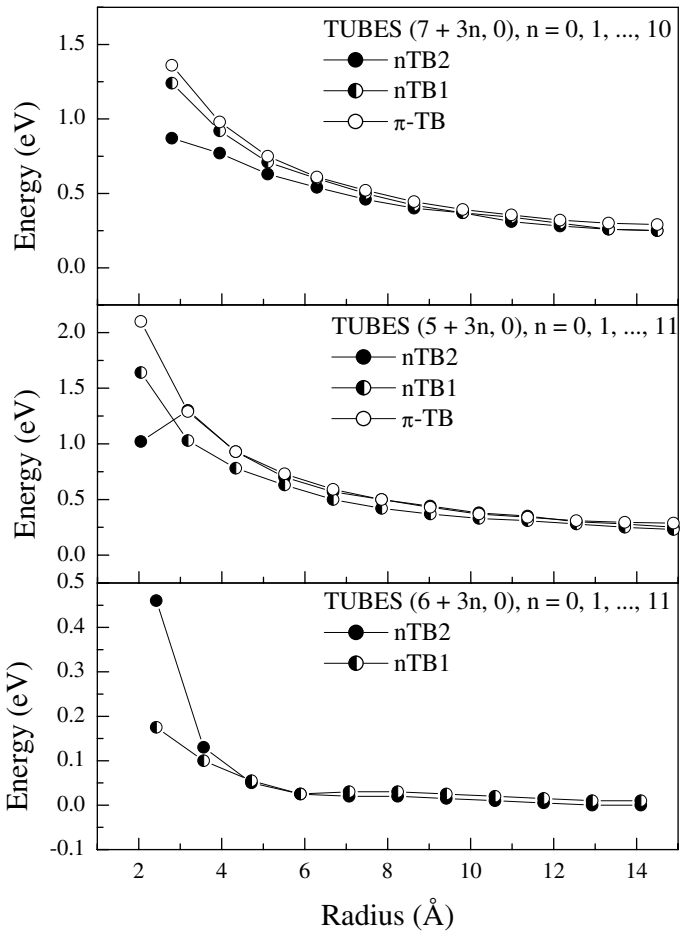

Figure 6. Calculated band gaps within the nTB model (nTB1: half-filled symbols; nTB2: filled symbols) versus tube radius R for all zigzag nanotubes in the range $2\,\text{Å} < R < 15\,\text{Å}$ in comparison with π-TB results for transfer integral $\gamma_0 = 2.75\,\text{eV}$ (open symbols).

model [4]. The calculations here show that the effects of the nanotube curvature on these energies have to be taken into account even for tubes with moderate radii.

5. Conclusions

The optimized structure, the electronic band structure and the dielectric function of a large number of small- and moderate-radius single-walled carbon nanotubes are studied within a non-orthogonal tight-binding model. The model is based on a symmetry-adapted scheme, which allows for significant reduction of the size of the matrix electronic eigenvalue problem. It is shown that the calculated electronic band structure of three small-radius nanotubes agrees well with *ab initio* simulations up to several eV above the Fermi energy and exhibits large differences with the π-TB results. Secondly, the dielectric function of many nanotubes is calculated within the random-phase approximation for energies up to 6 eV. The derived transition energies differ from the π-TB energies due to curvature effects. These differences are large for small radii and

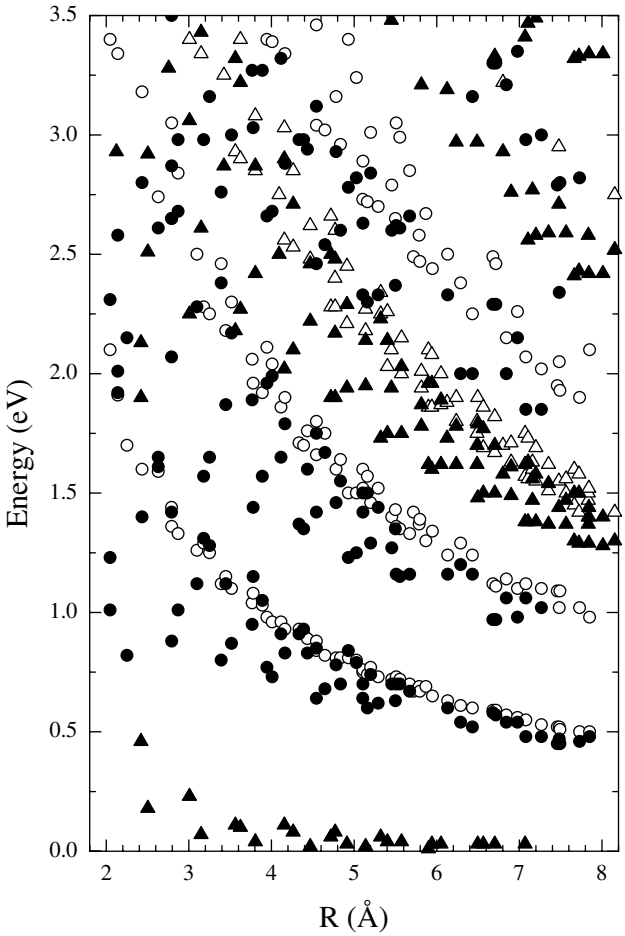

Figure 7. Calculated optical transition energies within the nTB2 model (filled symbols) for all nanotubes with radii between 2 and 8 Å and $N_c < 400$ in comparison with π-TB results for transfer integral $\gamma_0 = 2.75$ eV (open symbols).

decrease with increase in tube radius. The obtained transition energies versus nanotube radius can be used for the determination of the conditions for resonant Raman scattering from nanotubes.

Acknowledgments

This work was partly supported by a scholarship from the Belgian Federal Science Policy Office for promoting the S&T cooperation with Central and Eastern Europe, a NATO Collaborative Linkage Grant and a Marie-Curie Intra-European Fellowship. Stimulating discussions with L Henrard and A Rubio are acknowledged.

References

[1] Iijima S 1991 *Nature* **354** 56
[2] Mintmire J W, Dunlap B I and White C T 1992 *Phys. Rev. Lett.* **68** 631
[3] Hamada N, Sawada S and Oshiyama A 1992 *Phys. Rev. Lett.* **68** 1579

[4] Saito R, Fujita M, Dresselhaus G and Dresselhaus M S 1992 *Phys. Rev.* B **46** 1804
[5] Mintmire J W, Robertson D H and White C T 1993 *J. Phys. Chem. Solids* **54** 1835
[6] White C T, Robertson D H and Mintmire J W 1993 *Phys. Rev.* B **47** 5485
[7] Blase X, Benedict L X, Shirley E L and Louie S G 1994 *Phys. Rev. Lett.* **72** 1878
[8] Charlier J-C, Lambin Ph and Ebbesen T W 1996 *Phys. Rev.* B **54** R8377
[9] Reich S, Thomsen C and Ordejón P 2002 *Phys. Rev.* B **65** 155411
[10] Ajiki H and Ando T 1994 *Physica* B **201** 349
[11] Lin M F and Shung K W-K 1994 *Phys. Rev.* B **50** 17744
[12] Tasaki S, Maekawa K and Yamabe T 1998 *Phys. Rev.* B **57** 9301
[13] Milošević I, Vuković T, Dmitrović S and Damnjanović M 2003 *Phys. Rev.* B **67** 165418
[14] Mintmire J W and White C T 1996 *Synth. Met.* **77** 231
[15] Li Z M *et al* 2001 *Phys. Rev. Lett.* **87** 121401
[16] Machón M, Reich S, Thomsen C, Sánchez-Portal D and Ordejón P 2002 *Phys. Rev.* B **66** 155410
[17] Kataura H, Kumazawa Y, Maniwa Y, Umezu I, Suzuki S, Ohtsuka Y and Achiba Y 1999 *Synth. Met.* **103** 2555
[18] Hagen A and Hertel T 2003 *Nano Lett.* **3** 383
[19] Cao J X, Yan X H, Ding J W and Wang D L 2001 *J. Phys.: Condens. Matter* **13** L271
[20] Popov V N, Van Doren V E and Balkanski M 1999 *Phys. Rev.* B **59** 8355
[21] Popov V N, Van Doren V E and Balkanski M 2000 *Phys. Rev.* B **60** 3078
[22] Ehrenreich H and Cohen M H 1959 *Phys. Rev.* **115** 786
[23] Porezag D, Frauenheim Th and Köhler Th 1995 *Phys. Rev.* B **51** 12947
[24] Sánchez-Portal D, Artacho E, Soler J M, Rubio A and Ordejón P 1999 *Phys. Rev.* B **59** 12678
[25] Cabria I, Mintmire J W and White C T 2003 *Phys. Rev.* B **67** 121406
[26] Robertson D H, Brenner D W and Mintmire J W 1992 *Phys. Rev.* B **45** 12592
[27] Kürti J, Kresse G and Kuzmany H 1998 *Phys. Rev.* B **58** R8869
[28] Adams G, Sankey O, Page J, O'Keeffe M and Drabold D 1992 *Science* **256** 1792
[29] Jorio A, Pimenta M A, Souza Filho A G, Samsonidze Ge G, Swan A K, Ünlü M S, Goldberg B B, Saito R, Dresselhaus G and Dresselhaus M S 2003 *Phys. Rev. Lett.* **90** 107403
[30] Gülseren O, Yildirim T and Ciraci S 2002 *Phys. Rev.* B **65** 153405
[31] Ouyang M, Huang J, Cheung C L and Lieber C M 2001 *Science* **292** 702